The enigma of Neoproterozoic giant ooids—Fingerprints of extreme climate?

Elizabeth J. Trower[1]

[1]Department of Geological Sciences, University of Colorado Boulder, Boulder, CO, USA 80309.

Corresponding author: Elizabeth J. Trower (lizzy.trower@colorado.edu)

Key Points:

- Giant ooids are a rare carbonate facies that occur in strata underlying a number of Neoproterozoic glacial deposits.
- Giant ooid diameter was applied to constrain Neoproterozoic seawater carbonate saturation state, temperature, and alkalinity.
- Neoproterozoic giant ooids indicate hot or cold, but not moderate, climate at low latitudes preceding the onset of glaciations.

Abstract

Geologists have documented at least fourteen occurrences of "giant ooids", a geologically rare type of carbonate allochem, in Neoproterozoic successions at low paleo-latitudes. Recent experiments and modeling demonstrated that ooid size reflects an equilibrium between precipitation and abrasion rates, such that ooid size could be used as a geological proxy for $CaCO_3$ mineral saturation state (Ω). Here, the documented sizes of Neoproterozoic giant ooids were applied to estimate seawater Ω, which provided a novel constraint on temperature, partial pressure of CO_2, and alkalinity preceding Neoproterozoic glaciations. The results suggest that giant ooid formation was most plausible with seawater alkalinity elevated over its present value by at least a factor of two, and either much warmer (40°C) or much colder (0°C) climate than modern tropical carbonate platforms, which have important and divergent implications for climate states and ecosystem responses prior to the initiation of each Neoproterozoic glaciation.

Plain Language Summary

Ooids are a type of calcium carbonate sediment grain composed of a set of concentric layers formed around a small particle. Although most ooids are sand-size grains (<2 mm in diameter), rare cases, referred to as "giant ooids", are much larger, with some >1 cm in diameter. Geologists have suggested that these giant ooids reflected unusual seawater chemistry, but the exact conditions required for their formation remained unknown. Although giant ooids are geologically rare, a surprising number of occurrences have been described from Neoproterozoic rocks (1000-541 million years old) that underlie sedimentary layers deposited by low paleo-latitude glaciations (i.e., "Snowball Earth" events). This study used the grain diameters of Neoproterozoic ooids to estimate the temperature and composition of seawater when they formed. The results showed that Neoproterozoic seawater must have either been very hot or very cold just prior to these glaciations, a finding that challenges either climate models of this era or conceptual models of common modes of carbonate sediment formation and deposition.

1 Introduction

Neoproterozoic carbonate successions are host to enigmatic and geologically rare carbonate allochems known as "giant ooids", uncommonly large concentrically-coated carbonate grains (>2 mm in diameter). Sumner and Grotzinger (1993) noted that giant ooids occur more

commonly and were generally larger in diameter during Neoproterozoic time than any other period in Earth history; additional observations have confirmed this occurrence pattern (cf. Table 3 in Thorie et al., 2018). Geologists have speculated that the formation of giant ooids required exceptionally high calcium carbonate mineral saturation state and higher current velocities than are characteristic of modern ooid shoals (Sumner & Grotzinger, 1993; Swett & Knoll, 1989). Yet, this hypothesis has remained untested and does not clearly explain why giant ooids are not more common in older Precambrian successions.

Giant ooids have been documented in Neoproterozoic strata in Greenland, Svalbard, Canada, Alaska (USA), California (USA), Siberia, Mongolia, India, and Australia (Batten et al., 2004; Day et al., 2004; Fromhold & Wallace, 2011; Gutstadt, 1968; Macdonald, et al., 2009a, 2009b; Petrov, 2018; Singh, 1987; Srivastava, 2006; Sumner & Grotzinger, 1993; Swett & Knoll, 1989; Teitz & Mountjoy, 1989; Thorie et al., 2018; Trower & Grotzinger, 2010; Zenger, 1976). As was first noted by Grotzinger and James (2000), in almost every case, these giant ooids closely underly glacial diamictites and/or cap carbonates (Table 1) associated with one of the series of Neoproterozoic glacial episodes. The first two of these episodes occurred during the Cryogenian period and are known as “Snowball Earths” because geological evidence indicates widespread glaciation extending to low latitudes (Chumakov, 2007; Evans, 2000; Hoffman et al., 1998, 2017; Kirschvink, 1992; Trindade & Macouin, 2007). There is also evidence of a third glacial episode during the Ediacaran period, although it appears unlikely that it constituted a Snowball Earth due to the paucity of low-latitude glacial deposits (Hoffman & Li, 2009). The stratigraphic, and thus temporal, association of giant ooids with Neoproterozoic glacial deposits suggests that a better understanding of the thermal and geochemical conditions required for giant ooid formation would provide critical constraints for more robust models of the global carbon cycle and climate during this dynamic era.

Recent experiment and modeling demonstrated that ooid size reflects an equilibrium between precipitation and abrasion rates (Trower et al., 2017), with the implication that ooid size in the rock record can be used to infer the calcium carbonate mineral saturation state of ancient seawater, Ω, where $\Omega = \frac{[Ca^{2+}][CO_3^{2-}]}{K_{sp}}$ (K_{sp} is the solubility product constant). These reconstructed Ω values can then be applied to estimate the other parameters that describe the carbonate system: the partial pressure of CO_2 (pCO_2), alkalinity (ALK), pH, and the concentration of dissolved

inorganic carbon (DIC). Here, this approach is applied to Neoproterozoic giant ooids to provide a novel constraint on Neoproterozoic pCO_2, alkalinity, and temperature prior to the initiations of the Cryogenian Snowball Earths and the Ediacaran glaciation.

2 Methods

Based on the giant ooid occurrences documented by Sumner and Grotzinger (1993), with the addition of occurrences described more recently (Batten et al., 2004; Day et al., 2004; Fromhold & Wallace, 2011; Macdonald, et al., 2009a, 2009b; Petrov, 2018; Srivastava, 2006; Thorie et al., 2018; Trower & Grotzinger, 2010), Neoproterozoic giant ooids range from 2 to 25 mm in diameter (D) (Table 1). Within this range, D = 5 mm and D = 10 mm were chosen as representative grain sizes for which to assess characteristic Ω values—the former representative of a grain diameter observed in the majority of the giant ooid deposits and the latter a conservative representative of the largest ooids in these deposits (Table 1).

An equilibrium ooid size is the grain diameter, D_{eq}, at which the precipitation rate $R_{precipitation}$ and the abrasion rate $R_{abrasion}$ are equal (Trower et al., 2017). Abrasion rate can be estimated from the rock record by measuring D and determining a characteristic bed shear velocity, u_* (Trower et al., 2017). There are several potential approaches to estimating u_*: the simplest is to leverage the observation from modern systems that ooids are typically transported near the threshold of suspension and estimate u_* by assuming Rouse number P = 2.5, where $P = \frac{w_s}{\kappa u_*}$; κ = 0.41 is the von Kárman constant and w_s is settling velocity calculated following Dietrich (1982) with grain diameter (D), sediment density (ρ_s), fluid density (ρ_f), and fluid kinematic viscosity (ν). Alternatively, if bedforms are preserved in the rock record, their dimensions can be used to estimate u_* (Lapotre et al., 2017; Southard & Boguchwal, 1990). Because bedform dimensions are not well-documented for Neoproterozoic giant ooid occurrences, P = 2.5 was used to estimate a range for u_* corresponding to the range of giant ooid sizes (Figure S1). Consistent with this choice, most giant ooids have high sphericities, suggesting that they dominantly experienced collisional abrasion during saltation, rather than frictional abrasion during rolling and sliding (Sipos et al., 2018). $R_{abrasion}$ can then be calculated following Lamb et al. (2008) and Trower et al. (2017):

$$R_{abrasion} = \frac{\pi}{6}\frac{A_1 \rho_s Y w_i^3 D^3}{k_v \sigma_t^2 H_{fall}} \quad (1)$$

where σ_T is tensile strength and Y is Young's modulus of elasticity (1 MPa and 20 GPa, respectively, following Trower et al., 2017); w_i is impact velocity normal to the bed, calculated

following Lamb et al. (2008); H_{fall} is the typical height particles are transported above the bed, calculated following Lamb et al. (2008); $k_v = 9 \times 10^5$ is a non-dimensional constant calibrated for ooid abrasion by Trower et al. (2017); and $A_1 \approx 1/3$ (Sklar and Dietrich, 2004) accounts for the fact that the time between particle-bed impacts depends on the time for a particle to be transported from the bed up to H_{fall}, in addition to the time to settle back to the bed. H_{fall} and w_i both depend on water depth, H. H = 5 m was chosen as a representative water depth; sensitivity tests indicate that varying water depth has a negligible effect on the resulting Ω prediction (Figure S2). Application of this abrasion model relies on the assumptions (1) that ooid diminution primarily occurs through abrasion of mud-size (<62.5 μm) carbonate particles rather than fragmentation of larger particles, which is consistent with experimental observations of abrasion of carbonate sand (Trower et al., 2019) and limestone pebbles (Attal and Lavé, 2009), and (2) that abrasion rates calibrated for sand-size carbonate particles (Trower et al., 2017) can be extrapolated to pebble-size carbonate particles, which is supported by similarity in modeled rates with experimental rates for limestone pebbles (Attal and Lavé, 2009) (Figure S3).

For each combination of (D, u_*), one can estimate the precipitation rate required to sustain that D as the equilibrium ooid size: $R_{precipitation} = f \cdot R_{abrasion}$, where f = (0, 1] is intermittency of movement. For the purposes of this analysis, f = 0.01 (i.e., sediment is actively transported 1% of the time) was chosen as a lower bound on this parameter—resulting $R_{precipitation}$ estimates are therefore minimum values (Figure S4). This intermittency value is somewhat less than observed in modern ooid shoals—f = 0.1-0.25 on Ambergris shoal in the Turks and Caicos Islands (Trower et al., 2018)—but this infrequent active transport could be explained by the large heights and wavelengths characteristic of gravel bedforms (Carling, 1999). The value of Ω required for each D_{eq} can be solved for by rearranging the volumetric precipitation rate equation for the carbonate mineral of interest:

$$R_{precipitation} = k(\Omega - 1)^n \cdot \frac{M}{\rho_s} \cdot A_{surface} \quad (2)$$

where k is the rate constant (μmol/m^2/hr), n is the reaction order (dimensionless), M is the molar mass of the calcium carbonate mineral (g/mol), and $A_{surface}$ is the ooid surface area (m^2).

Four scenarios with different mineralogy and/or temperature were simulated, using estimates for seawater density and kinematic viscosity as a function of temperature (T) and salinity (S) (Nayar et al., 2016; Sharqawy et al., 2010): (1) giant ooids composed of aragonite under conditions similar to modern carbonate platforms (T = 25°C, S = 35 ppt, ρ_s = 2800 kg/m^3, ρ_f = 1025 kg/m^3, ν_f = 9.37 x 10^{-7} m^2/s); (2) giant ooids composed of calcite (ρ_s = 2700 kg/m^3) under the same conditions as (1); (3) giant ooids composed of aragonite under warmer climate (T = 40°C, S = 35 ppt, ρ_f = 1018 kg/m^3, ν_f = 6.95 x 10^{-7} m^2/s); and (4) giant ooids composed of ikaite (T = 0°C, S = 50 ppt, ρs = 1800, ρ_f = 1040 kg/m^3, ν_f = 1.89 x 10^{-6} m^2/s). Ikaite is a hydrated calcium carbonate mineral ($CaCO_3 \cdot 6H_2O$) that precipitates only at cold temperatures (< 4°C) and rapidly dehydrates to monohydrated calcite, calcite, aragonite, or vaterite at warmer temperatures (timescales of hours to days) (Bischoff et al., 1993a; Ito, 1998; Shaikh, 1990; Tang et al., 2009) or after any subaerial exposure (Smoot & Lowenstein, 1991). The latter scenarios were predicted to be more amenable to larger equilibrium ooid sizes, either due to higher precipitation rate at a warmer temperature or due to lower abrasion rate resulting from the low density of ikaite and high viscosity of cold seawater. Kinetic parameters for aragonite and calcite precipitation at 25°C, aragonite at 40°C, and ikaite at 0°C were after Zhong and Mucci (1989), Burton and Walter (1987), and Papadimitriou et al. (2014), respectively. Results for aragonite and calcite at T = 0°C were not included in the following analysis because their sluggish precipitation kinetics at low temperature (Burton & Walter, 1987; Lopez et al., 2009) make them an implausible alternative to ikaite (Figure S5).

PHREEQC (Parkhurst & Appelo, 2013) was used to estimate combinations of pCO_2 and ALK required for the Ω values determined for each of the four scenarios (Supplementary Text S1). A range of alkalinity from 2 to 10 meq/L and a range of pCO_2 from $10^{-2.5}$ to 10^{-5} atm were explored. The PHREEQC database (Parkhurst & Appelo, 2013) was applied for aragonite/calcite at T = 25°C, 40°C and the FREZCHEM database (Marion et al., 2010) was applied for ikaite at T = 0°C. The concentration of Ca^{2+} was constrained as a function of alkalinity, with either Ca:ALK = 5 (i.e., modern seawater) or Ca:ALK = 0.75, the minimum estimate from Blattler et al. (2016); and the concentration of Mg^{2+} was constrained as a function of [Ca^{2+}], with either Mg:Ca = 1 or Mg:Ca = 5, following endmember values from Hardie (2003).

3 Results

159 The carbonate mineral saturation states required for giant ooids with D = 10 mm varied
160 substantially depending on mineralogy (aragonite, calcite, or ikaite) and temperature (T = 0°C,
161 25°C, 40°C) (Figure 1). Aragonitic or calcitic ooids of this size under conditions similar to those
162 on modern carbonate platforms (i.e., T = 25°C) required $\Omega_{aragonite} \cong 19$ or $\Omega_{calcite} \cong 26$ (Figure
163 1a-b), both of which are notably higher than saturation states observed in modern shallow marine
164 settings (e.g., $\Omega_{aragonite} = 5$ in the Turks and Caicos Islands, Trower et al., 2018). In contrast,
165 aragonitic giant ooids at T = 40°C required $\Omega_{aragonite} \cong 10$ (Figure 1c) and ikaite giant ooids at T
166 = 0°C required $\Omega_{ikaite} \cong 4$ (Figure 1d). Smaller giant ooids (D = 5 mm) required lower saturation
167 states—$\Omega_{aragonite} \cong 12$ or $\Omega_{calcite} \cong 17$ for T = 25°C, $\Omega_{aragonite} \cong 7$ for T = 40°C, or $\Omega_{ikaite} \cong 2$ for
168 T = 0°C. PHREEQC results illustrated that all cases required ALK > 2 meq/L and $pCO_2 \leq 10^{-2.5}$
169 atm (~10x present atmospheric level, PAL) (Figure 2); the lowest minimum ALK values were
170 associated with Ca:ALK = 5. Mg:Ca = 5 cases required higher alkalinity and lower pCO_2 than
171 Mg:Ca = 1 cases. The ikaite scenario required somewhat higher ALK and lower pCO_2 than the
172 other scenarios because ikaite is more soluble than aragonite or calcite.

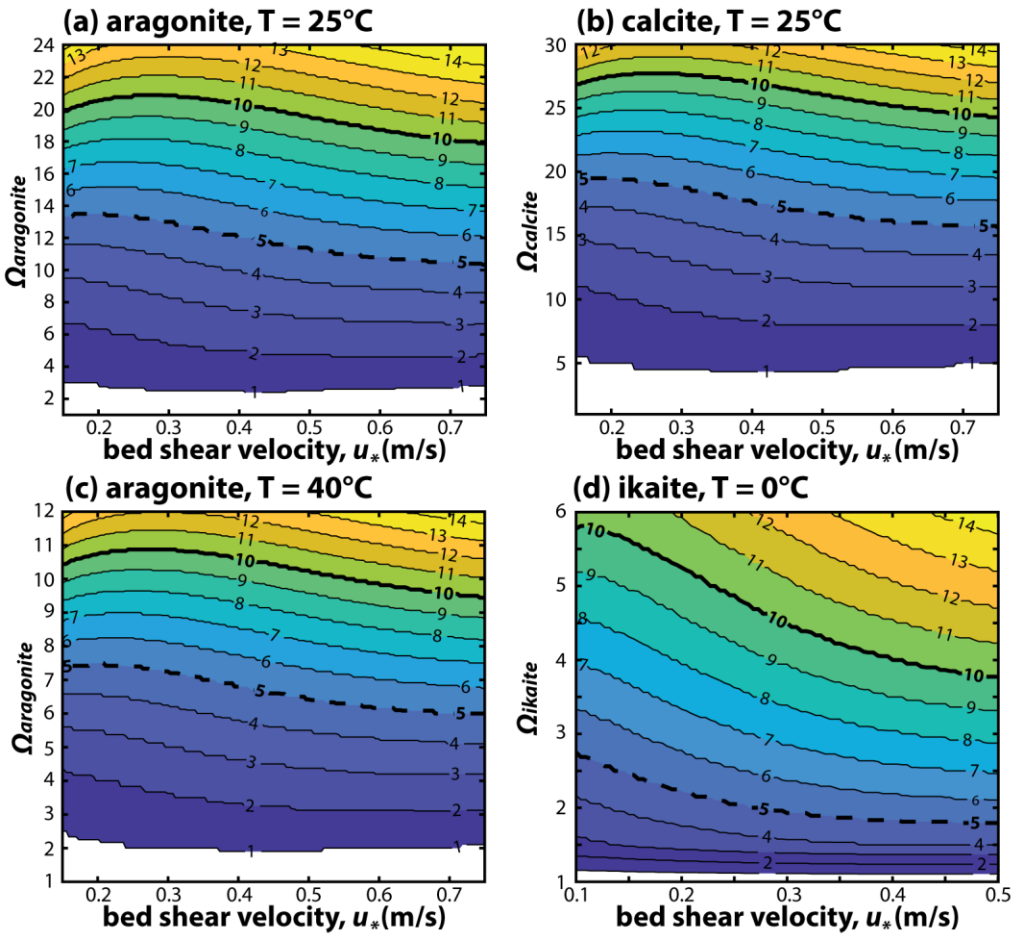

Figure 1. Contour plots of equilibrium ooid size (mm) as a function of carbonate mineral saturation state (Ω) vs. bed shear velocity (u_*) for four scenarios: (a) aragonite giant ooids at T = 25°C, (b) calcite giant ooids at T = 25°C, (c) aragonite giant ooids at T = 40°C, and (d) ikaite at 0°C. Solid bold lines indicate combinations of Ω and u_* consistent with D_{eq} = 10 mm; dashed bold lines indicate combinations of Ω and u_* consistent with D_{eq} = 5 mm. The range in u_* in each plot is consistent with P = 2.5 for grain sizes ranging from 1-10 mm (Figure S1). Notably, D_{eq} is more sensitive to Ω than u_* in all cases, so an exact constraint on u_* is not necessary to estimate Ω.

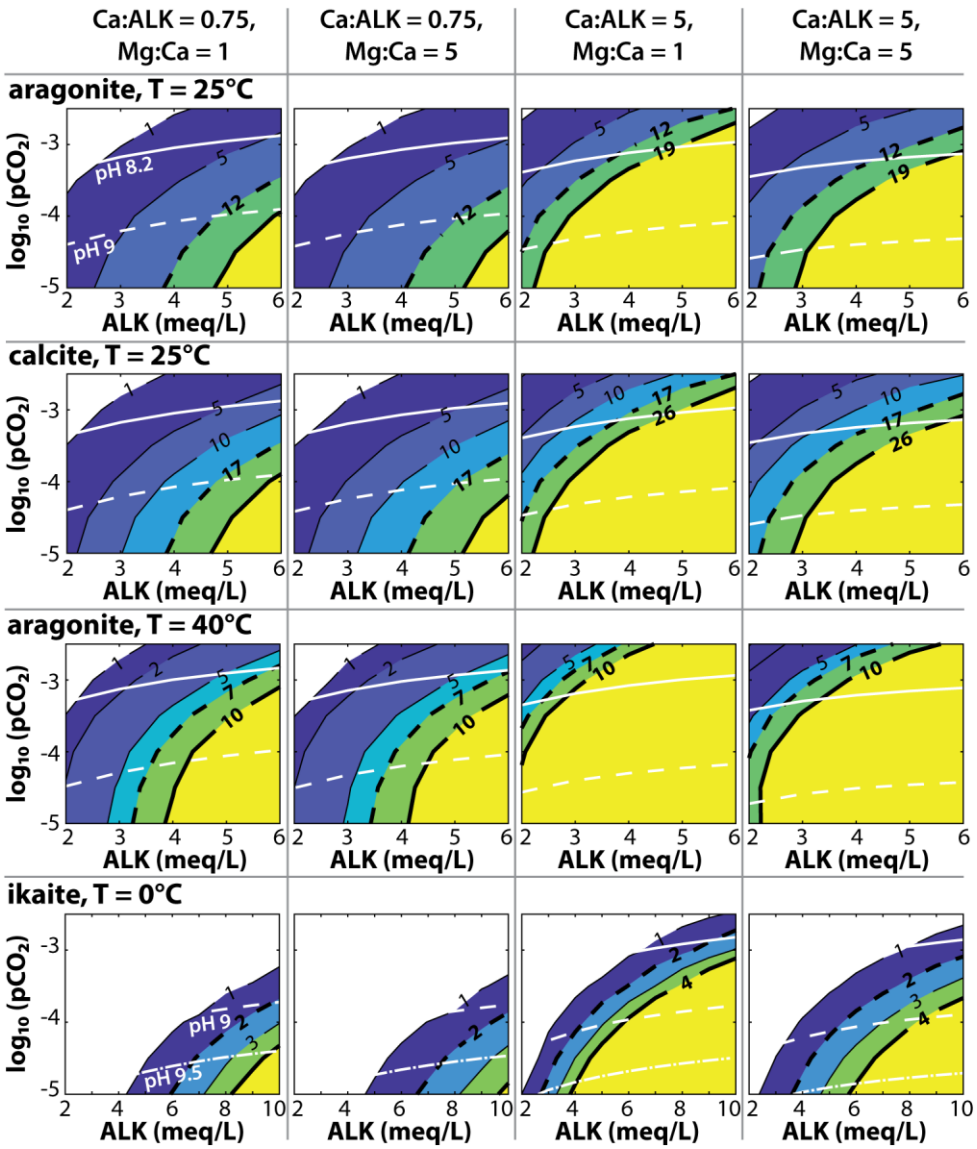

Figure 2. Contour plots of Ω as a function of $\log_{10}(pCO_2)$ vs. ALK for each of the four scenarios with Ca:ALK = 0.75 or 5 and Mg:Ca = 1 or 5. In each row, the solid bold black line indicates the Ω value necessary for D_{eq} = 10 mm and the dashed bold black line indicates the Ω value necessary for D_{eq} = 5 mm. The white lines indicate contours of pH = 8.2 (solid line), pH = 9 (dashed line), and pH = 9.5 (dash-dot line). pH = 8.2 is used as a benchmark following boron isotope constraints from Kasemann et al. (2010).

4 Discussion

The combination of elevated ALK and relatively low pCO_2 indicated in all scenarios (Figure 2) is consistent with drawdown of CO_2 and increased seawater alkalinity due to enhanced weathering prior to the Snowball glaciations (Cox et al., 2016; Donnadieu et al., 2004; Goddéris et al., 2003; Hoffman et al., 1998). However, not all scenarios are equally plausible. Although Neoproterozoic carbonate successions have been interpreted to have formed under conditions similar to modern tropical carbonate platforms (e.g., Hoffman et al., 1998), the high Ω values implied by the 25°C scenarios are not particularly plausible solutions. It is unlikely that the Ω values required for D = 10 mm ($\Omega_{aragonite} \cong 19$ or $\Omega_{calcite} \cong 26$) could be sustained over the >1000 year timescales necessary for ooid growth (Beaupré et al., 2015; Duguid et al., 2010). Both Ω values are above the thresholds for homogeneous nucleation of aragonite or calcite, respectively (Morse & He, 1993; Pokrovsky, 1998; Sun et al., 2015); at these Ω values, the respective carbonate mineral would have nucleated rapidly both on available surfaces (heterogeneous nucleation)—including ooid surfaces, particular organic matter, etc.—and spontaneously within the water column (homogeneous nucleation). Furthermore, the rapid $CaCO_3$ nucleation/precipitation at high Ω values and the relatively slow rate of CO_2 hydration/hydroxylation (Zeebe & Wolf-Gladrow, 2001) would both provide strong negative feedbacks on Ω. Although the T = 25°C $\Omega_{aragonite}$ or $\Omega_{calcite}$ values for D = 5 mm are more plausible from this perspective, they are not consistent with the observations of ooids with $D > 5$ mm. Based on the common occurrence of giant ooids with diameters ≥ 10 mm, it is therefore more likely that Neoproterozoic giant ooids formed under conditions that were either much warmer (T = 40°C) or much colder (T = 0°C) than modern carbonate platforms.

The juxtaposition of 40°C seawater with a geochemical signature of the climate changes leading to Snowball initiation (i.e., elevated alkalinity and relatively low pCO_2) is surprising, even considering the relatively low paleo-latitudes of Cryogenian giant ooid-bearing strata (Table 1). Due to the reduced solar luminosity during Neoproterozoic time relative to the present (Gough, 1981), models with $pCO_2 \cong 10^{-2.7}$ atm have predicted a cooler-than-modern climate, and that $pCO_2 \lesssim$ PAL was sufficiently low to trigger global glaciation (Donnadieu et al., 2004; Hyde et al., 2000; Micheels & Montenari, 2008; Pierrehumbert et al., 2011). Temperatures ≥ 40°C at low latitudes are consistent with models of post-Snowball greenhouse climate (Le Hir et al., 2009; Pierrehumbert et al., 2011; Yang et al., 2017), although these models require $pCO_2 \cong$ 400x

PAL (~$10^{-0.9}$ atm), implying ALK >> 6 meq/L (Figure 2). Although the occurrences of giant ooids that stratigraphically underlie end-Cryogenian glacial deposits could be consistent (and indicative) of the persistence of greenhouse conditions after the early-Cryogenian and end-Cryogenian Snowball Earths, this mechanism cannot explain the occurrences of giant ooids that stratigraphically underlie the early-Cryogenian glacial deposits because there is no preceding Snowball. Based on these climate models, the T = 40°C scenario is probably only plausible for $pCO_2 \geq$ the maximum value modeled ($10^{-2.5}$ atm), implying pH < 8.2, which conflicts with the pH constraint from boron isotopes (Kasemann et al., 2010). Furthermore, this scenario implies that, prior to the early-Cryogenian Snowball Earth, low-latitude climate was warmer and pCO_2 was higher than climate models can currently account for.

Although the cold scenario requires higher ALK (6-10 meq/L) and lower pCO_2 (~10^{-4}) than other cases, it is consistent with several lines of evidence from the rock record. Glendonite—a pseudomorph of ikaite—has been reported in Cryogenian (James et al., 2005) and Ediacaran (Wang et al., 2017) carbonate units deposited prior to glaciogenic sediments; in the former case, glendonites are described in close stratigraphic association with giant ooids. Ooids formed in cold-water conditions have also been observed adjacent to glaciers in Antarctica (Goodwin et al., 2018; Rao et al., 1998) and in Cryogenian carbonates interpreted as glaciolacustrine deposits (Fairchild et al., 2016), although neither case has been definitively identified as having initially precipitated as ikaite. Furthermore, there is reason to suspect that ikaite might be substantially under-recognized in the rock record due to its rapid transformation to calcite and aragonite at temperatures only modestly above 0°C or after subaerial exposure. Analysis of modern and Holocene carbonates in lakes in California and Patagonia has suggested that most of this carbonate originally precipitated as ikaite before transforming to calcite or aragonite during warmer seasons (Bischoff, et al., 1993b; Council & Bennett, 1993; Oehlerich et al., 2013). In these cases, ikaite had not been recognized as the dominant primary phase until identified via analyses of modern samples because the crystal size of much of the primary ikaite was much smaller than the characteristic glendonite pseudomorphs. This scenario, if correct, implies that Neoproterozoic giant ooids are an indicator facies of cold conditions at low-latitudes prior to the delivery of glacially-derived sediment, with the consequence that strata associated with giant ooids could provide a record of ecosystem responses to this extreme cooling. Notably,

formation of ooids of any size also requires current transport, so this scenario would also require areas of open water in order for waves to interact with the seafloor.

The results presented here illustrate that Neoproterozoic giant ooids must be reconciled with at least one surprising finding: the T = 25°C scenarios require seawater Ω sustained at extremely and likely implausibly high values; the T = 40°C scenario requires a hot, high pCO_2 climate not long before the initiation of each Neoproterozoic glaciation, which could be consistent with the persistence of a post-Snowball greenhouse, but is problematic as an explanation for giant ooids that precede the oldest Neoproterozoic Snowball; and finally, the T = 0°C scenario requires an original primary mineralogy that is currently considered geologically rare and suggests that low latitude seawater was already cold prior to the onset of glacially-derived sediment deposition. Future work focused on improving our ability to recognize the diagenetic products of fine-grained ikaite and modeling pre-glacial climate will enable more robust tests of the hot pre-glacial seawater vs. cold syn-glacial giant ooid scenarios. Regardless, these results demonstrate that giant ooids are not merely a geologic curiosity, but a key indicator of uncommon carbonate chemistry and climate. The finding that giant ooid formation is most plausible at extreme temperatures—in addition to requiring high alkalinity and strong currents necessary to transport large particles—may finally explain why they are so uncommon in the rock record.

Acknowledgments, Samples, and Data

The author thanks Carl Simpson and Miquela Ingalls for helpful discussions. Data supporting the conclusions are provided in the figures, table, supplementary information, and cited references. Matlab code used to calculate equilibrium ooid sizes is archived at:
https://doi.org/10.5281/zenodo.3531994

References

Attal, M., & Lavé, J. (2009). Pebble abrasion during fluvial transport: Experimental results and implications for the evolution of the sediment load along rivers. Journal of Geophysical Research, 114(F4), 607.

277 Batten, K. L., Narbonne, G. M., & James, N. P. (2004). Paleoenvironments and growth of early
278 Neoproterozoic calcimicrobial reefs: platformal Little Dal Group, northwestern Canada.
279 Precambrian Research, 133(3), 249–269.

280 Beaupré, S. R., Roberts, M. L., Burton, J. R., & Summons, R. E. (2015). Rapid, high-resolution
281 14C chronology of ooids. Geochimica et Cosmochimica Acta, 159, 126–138.

282 Bischoff, J. L., Fitzpatrick, J. A., & Rosenbauer, R. J. (1993a). The Solubility and Stabilization
283 of ikaite (CaCO3-6H20) from 0° to 25°C: Environmental and Paleoclimatic: Implications
284 for Thinolite Tufa. The Journal of Geology, 101, 21–33.

285 Bischoff, J. L., Stine, S., Rosenbauer, R. J., Fitzpatrick, J. A., & Stafford, T. W. (1993b). Ikaite
286 precipitation by mixing of shoreline springs and lake water, Mono Lake, California,
287 USA. Geochimica et Cosmochimica Acta, 57(16), 3855–3865.

288 Blättler, C. L., Kump, L. R., Fischer, W. W., Paris, G., Kasbohm, J. J., & Higgins, J. A. (2016).
289 Constraints on ocean carbonate chemistry and pCO2 in the Archaean and
290 Palaeoproterozoic. Nature Geoscience, 10, 41.

291 Burton, E. A., & Walter, L. M. (1987). Relative precipitation rates of aragonite and Mg calcite
292 from seawater: Temperature or carbonate ion control? Geology, 15, 111–114.

293 Carling, P. A. (1999). Subaqueous gravel dunes. Journal of Sedimentary Research, 69(3), 534–
294 545.

295 Chumakov, N. M. (2007). Climates and climate zonality of the Vendian: geological evidence.
296 Geological Society, London, Special Publications, 286(1), 15–26.

297 Council, T. C., & Bennett, P. C. (1993). Geochemistry of ikaite formation at Mono Lake,
298 California: Implications for the origin of tufa mounds. Geology, 21(11), 971–974.

299 Cox, G. M., Halverson, G. P., Stevenson, R. K., Vokaty, M., Poirier, A., Kunzmann, M., et al.
300 (2016). Continental flood basalt weathering as a trigger for Neoproterozoic Snowball
301 Earth. Earth and Planetary Science Letters, 446, 89–99.

302 Day, E. S., James, N. P., Narbonne, G. M., & Dalrymple, R. W. (2004). A sedimentary prelude
303 to Marinoan glaciation, Cryogenian (Middle Neoproterozoic) Keele Formation,
304 Mackenzie Mountains, northwestern Canada. Precambrian Research, 133(3), 223–247.

Dietrich, W. E. (1982). Settling velocity of natural particles. Water Resources Research, 18(6), 1615–1626.

Donnadieu, Y., Goddéris, Y., Ramstein, G., Nédélec, A., & Meert, J. (2004). A "snowball Earth" climate triggered by continental break-up through changes in runoff. Nature, 428(6980), 303–306.

Duguid, S. M. A., Kurtis Kyser, T., James, N. P., & Rankey, E. C. (2010). Microbes and Ooids. Journal of Sedimentary Research, 80(3), 236–251.

Evans, D. A. D. (2000). Stratigraphic, geochronological, and paleomagnetic constraints upon the Neoproterozoic climatic paradox. American Journal of Science, 300(5), 347–433.

Fairchild, I. J., Fleming, E. J., Bao, H., Benn, D. I., Boomer, I., Dublyansky, Y. V., et al. (2016). Continental carbonate facies of a Neoproterozoic panglaciation, north-east Svalbard. Sedimentology, 63(2), 443–497.

Fromhold, T. A., & Wallace, M. W. (2011). Nature and significance of the Neoproterozoic Sturtian–Marinoan Boundary, Northern Adelaide Geosyncline, South Australia. Australian Journal of Earth Sciences, 58(6), 599–613.

Goddéris, Y., Donnadieu, Y., Nédélec, A., Dupré, B., Dessert, C., Grard, A., et al. (2003). The Sturtian "snowball" glaciation: fire and ice. Earth and Planetary Science Letters, 211(1), 1–12.

Goodwin, I. D., Roberts, J. L., & Etheridge, D. M. (2018). Modern to Glacial age subglacial meltwater drainage at Law Dome, coastal East Antarctica from topography, sediments and jökulhlaup observations. Geological Society. Retrieved from https://sp.lyellcollection.org/content/461/1/215.abstract

Gough, D. O. (1981). Solar Interior Structure and Luminosity Variations. In Physics of Solar Variations (pp. 21–34). Springer Netherlands.

Grotzinger, J. P., & James, N. P. (2000). Precambrian carbonates: evolution of understanding. In J. P. Grotzinger & N. P. James (Eds.), Carbonate Sedimentation and Diagenesis in the Evolving Precambrian World (Vol. 67, pp. 3–20). SEPM Special Publication.

Gutstadt, A. M. (1968). Petrology and depositional environments of the Beck Spring Dolomite (Precambrian), Kingston Range, California. Journal of Sedimentary Petrology, 38(4), 1280–1289.

Hardie, L. A. (2003). Secular variations in Precambrian seawater chemistry and the timing of Precambrian aragonite seas and calcite seas. Geology, 31(9), 785–788.

Hoffman, P. F., & Li, Z.-X. (2009). A palaeogeographic context for Neoproterozoic glaciation. Palaeogeography, Palaeoclimatology, Palaeoecology, 277(3), 158–172.

Hoffman, P. F., Kaufman, A. J., Halverson, G. P., & Schrag, D. P. (1998). A neoproterozoic snowball earth. Science, 281(5381), 1342–1346.

Hoffman, P. F., Abbot, D. S., Ashkenazy, Y., Benn, D. I., Brocks, J. J., Cohen, P. A., et al. (2017). Snowball Earth climate dynamics and Cryogenian geology-geobiology. Science Advances, 3(11), e1600983.

Hyde, W. T., Crowley, T. J., Baum, S. K., & Peltier, W. R. (2000). Neoproterozoic "snowball Earth" simulations with a coupled climate/ice-sheet model. Nature, 405(6785), 425–429.

Ito, T. (1998). Factors controlling the transformation of natural ikaite from Shiowakka, Japan. Geochemical Journal, 32, 267–273.

James, N. P., Narbonne, G. M., Dalrymple, R. W., & Kurtis Kyser, T. (2005). Glendonites in Neoproterozoic low-latitude, interglacial, sedimentary rocks, northwest Canada: Insights into the Cryogenian ocean and Precambrian cold-water carbonates. Geology, 33(1), 9–12.

Kasemann, S. A., Prave, A. R., Fallick, A. E., Hawkesworth, C. J., & Hoffmann, K.-H. (2010). Neoproterozoic ice ages, boron isotopes, and ocean acidification: Implications for a snowball Earth. Geology, 38(9), 775–778.

Kirschvink, J. L. (1992). Late Proterozoic Low-Latitude Global Glaciation: the Snowball Earth. In J. W. Schopf & C. Klein (Eds.), The Proterozoic biosphere : a multidisciplinary study (pp. 51–52). New York: Cambridge University Press.

Lamb, M. P., Dietrich, W. E., & Sklar, L. S. (2008). A model for fluvial bedrock incision by impacting suspended and bed load sediment. Journal of Geophysical Research, 113(F3), 225.

Lapotre, M. G. A., Lamb, M. P., & McElroy, B. (2017). What sets the size of current ripples? Geology, 45(3), 243–246.

Le Hir, G., Donnadieu, Y., Goddéris, Y., Pierrehumbert, R. T., Halverson, G. P., Macouin, M., et al. (2009). The snowball Earth aftermath: Exploring the limits of continental weathering processes. Earth and Planetary Science Letters, 277(3), 453–463.

Lopez, O., Zuddas, P., & Faivre, D. (2009). The influence of temperature and seawater composition on calcite crystal growth mechanisms and kinetics: Implications for Mg incorporation in calcite lattice. Geochimica et Cosmochimica Acta, 73(2), 337–347.

Macdonald, F. A., Jones, D. S., & Schrag, D. P. (2009a). Stratigraphic and tectonic implications of a newly discovered glacial diamictite–cap carbonate couplet in southwestern Mongolia. Geology, 37(2), 123–126.

Macdonald, F. A., McClelland, W. C., Schrag, D. P., & Macdonald, W. P. (2009b). Neoproterozoic glaciation on a carbonate platform margin in Arctic Alaska and the origin of the North Slope subterrane. GSA Bulletin, 121(3-4), 448–473.

Marion, G. M., Mironenko, M. V., & Roberts, M. W. (2010). FREZCHEM: A geochemical model for cold aqueous solutions. Computers & Geosciences, 36(1), 10–15.

Micheels, A., & Montenari, M. (2008). A snowball Earth versus a slushball Earth: Results from Neoproterozoic climate modeling sensitivity experiments. Geosphere, 4(2), 401–410.

Morse, J. W., & He, S. (1993). Influences of T, S and PCO2 on the pseudo-homogeneous precipitation of CaCO3 from seawater: implications for whiting formation. Marine Chemistry, 41(4), 291–297.

Nayar, K. G., Sharqawy, M. H., Banchik, L. D., & Lienhard, J. H., V. (2016). Thermophysical properties of seawater: A review and new correlations that include pressure dependence. Desalination, 390, 1–24.

Oehlerich, M., Mayr, C., Griesshaber, E., Lücke, A., Oeckler, O. M., Ohlendorf, C., et al. (2013). Ikaite precipitation in a lacustrine environment – implications for palaeoclimatic studies using carbonates from Laguna Potrok Aike (Patagonia, Argentina). Quaternary Science Reviews, 71, 46–53.

Papadimitriou, S., Kennedy, H., Kennedy, P., & Thomas, D. N. (2014). Kinetics of ikaite precipitation and dissolution in seawater-derived brines at sub-zero temperatures to 265K. Geochimica et Cosmochimica Acta, 140, 199–211.

Parkhurst, D. L., & Appelo, C. A. J. (2013). Description of Input and Examples for PHREEQC Version 3—A Computer Program for Speciation, Batch-Reaction, One-Dimensional Transport, and Inverse Geochemical Calculations (No. Techniques and Methods 6–A43). USGS. Retrieved from https://pubs.usgs.gov/tm/06/a43/pdf/tm6-A43.pdf

Pelechaty, S. M. (1998). Integrated chronostratigraphy of the Vendian System of Siberia: implications for a global stratigraphy. Journal of the Geological Society, 155(6), 957–973.

Petrov, P. Y. (2018). Postglacial Deposits of the Dal'nyaya Taiga Group: Early Vendian in the Ura Uplift, Siberia. Communication 2. Ura and Kalancha Formations and History of the Basin. Lithology and Mineral Resources, 53(6), 473–488.

Pierrehumbert, R. T., Abbot, D. S., Voigt, A., & Koll, D. (2011). Climate of the Neoproterozoic. Annual Review of Earth and Planetary Sciences, 39(1), 417–460.

Pokrovsky, O. S. (1998). Precipitation of calcium and magnesium carbonates from homogeneous supersaturated solutions. Journal of Crystal Growth, 186(1), 233–239.

Rao, C. P., Goodwin, I. D., & Gibson, J. A. E. (1998). Shelf, coastal and subglacial polar carbonates, East Antarctica. Carbonates and Evaporites, 13(2), 174–188.

Shaikh, A. M. (1990). A new crystal growth form of vaterite, CaCO3. Journal of Applied Crystallography. Retrieved from https://scripts.iucr.org/cgi-bin/paper?gl0147

Sharqawy, M. H., Lienhard, J. H., & Zubair, S. M. (2010). Thermophysical properties of seawater: a review of existing correlations and data. Desalination and Water Treatment, 16(1-3), 354–380.

Singh, U. (1987). Ooids and cements from the late Precambrian of the Flinders Ranges, South Australia. Journal of Sedimentary Petrology, 57(1), 117–127.

Sipos, A. A., Domokos, G., & Jerolmack, D. J. (2018). Shape evolution of ooids: a geometric model. Scientific Reports, 8(1), 1758.

Sklar, L. S., & Dietrich, W. E. (2004). A mechanistic model for river incision into bedrock by saltating bed load. Water Resources Research, 40(6).

Smoot, J. P., & Lowenstein, T. K. (1991). Depositional Environments of Non-Marine Evaporites. In J. L. Melvin (Ed.), Evaporites, Petroleum and Mineral Resources (Vol. 50, pp. 189–348). Amsterdam: Elsevier.

Southard, J. B., & Boguchwal, L. A. (1990). Bed configuration in steady unidirectional water flows; Part 2, Synthesis of flume data. Journal of Sedimentary Research, 60(5), 658–679.

Srivastava, P. (2006). Meso–Neoproterozoic coated grains and palaeoecology of associated microfossils: The Deoban Limestone, Lesser Himalaya, India. Palaeogeography, Palaeoclimatology, Palaeoecology, 239(3), 241–252.

Sumner, D. Y., & Grotzinger, J. P. (1993). Numerical modeling of ooid size and the problem of Neoproterozoic giant ooids. Journal of Sedimentary Petrology, 63(5), 974–982.

Sun, W., Jayaraman, S., Chen, W., Persson, K. A., & Ceder, G. (2015). Nucleation of metastable aragonite CaCO3 in seawater. Proceedings of the National Academy of Sciences of the United States of America, 112(11), 3199–3204.

Swett, K., & Knoll, A. H. (1989). Marine pisolites from Upper Proterozoic carbonates of East Greenland and Spitsbergen. Sedimentology, 36, 75–93.

Tang, C. C., Thompson, S. P., Parker, J. E., Lennie, A. R., Azough, F., & Kato, K. (2009). The ikaite-to-vaterite transformation: new evidence from diffraction and imaging. Journal of Applied Crystallography, 42(2), 225–233.

Teitz, M., & Mountjoy, E. W. (1989). The late Proterozoic Yellowhead carbonate platform west of Jasper, Alberta. In H. H. J. Geldsetzer, N. P. James, & G. E. Tebbun (Eds.), Reefs, Canada and Adjacent Area (Vol. 13, pp. 129–134). Canadian Society of Petroleum Geologists.

Thorie, A., Mukhopadhyay, A., Banerjee, T., & Mazumdar, P. (2018). Giant ooids in a Neoproterozoic carbonate shelf, Simla Group, Lesser Himalaya, India: An analogue related to Neoproterozoic glacial deposits. Marine and Petroleum Geology, 98, 582–606.

Trindade, R. I. F., & Macouin, M. (2007). Palaeolatitude of glacial deposits and palaeogeography of Neoproterozoic ice ages. Comptes Rendus: Geoscience, 339(3), 200–211.

Trower, E. J., & Grotzinger, J. P. (2010). Sedimentology, diagenesis, and stratigraphic occurrence of giant ooids in the Ediacaran Rainstorm Member, Johnnie Formation, Death Valley region, California. Precambrian Research, 180(1-2), 113–124.

Trower, E. J., Lamb, M. P., & Fischer, W. W. (2017). Experimental evidence that ooid size reflects a dynamic equilibrium between rapid precipitation and abrasion rates. Earth and Planetary Science Letters, 468, 112–118.

Trower, E. J., Cantine, M. D., Gomes, M. L., Grotzinger, J. P., Knoll, A. H., Lamb, M. P., et al. (2018). Active Ooid Growth Driven By Sediment Transport in a High-Energy Shoal, Little Ambergris Cay, Turks and Caicos Islands. Journal of Sedimentary Research, 88(9), 1132–1151.

Trower, E. J., Lamb, M. P., & Fischer, W. W. (2019). The origin of carbonate mud. Geophysical Research Letters, 46(5), 2696–2703.

Wang, Z., Wang, J., Suess, E., Wang, G., Chen, C., & Xiao, S. (2017). Silicified glendonites in the Ediacaran Doushantuo Formation (South China) and their potential paleoclimatic implications. Geology, 45(2), 115–118.

Yang, J., Jansen, M. F., Macdonald, F. A., & Abbot, D. S. (2017). Persistence of a freshwater surface ocean after a snowball Earth. Geology, 45(7), 615–618.

Zeebe, R. E., & Wolf-Gladrow, D. (2001). CO2 in Seawater: Equilibrium, Kinetics, Isotopes (Vol. 65). Amsterdam: Elsevier.

Zenger, D. H. (1976). Dolomitization and dolomite “dikes” in the Wyman Formation (Precambrian), Northeastern Inyo Mountains, California. Journal of Sedimentary Petrology, 46(3), 457–462.

Zhong, S., & Mucci, A. (1989). Calcite and aragonite precipitation from seawater solutions of various salinities: Precipitation rates and overgrowth compositions. Chemical Geology, 78(3-4), 283–299.

471 **Table 1.** Neoproterozoic giant ooid-bearing strata and their relationship with glacial deposits.

472

Giant-ooid-bearing unit	Grain diameters (mm)[a]	Overlying glacial unit (associated glaciation: early-Cryogenian, end-Cryogenian, Ediacaran)	Paleolatitude range[b]	Reference(s)
Backlundtoppen Formation (Svalbard)	4-9 (maximum 14)	Elbobreen Formation, Petrovbreen Member (early-Cryogenian), not directly overlying	S 15-30°	Swett and Knoll (1989)
Beck Spring Dolomite (California, USA)	≤ 10	Kingston Peak Formation, Surprise Diamictite equivalent (early-Cryogenian)	N 0-15°	Gutstadt (1968)
Grainstone Formation, Little Dal Group (NW Canada)	2-10	Rapitan Group (early-Cryogenian)	N 0-15°	Batten et al. (2004)
Deoban Limestone (Lesser Himalaya, India)	≤ 6[c]	Blaini Group (end-Cryogenian)	N 0-15°	Srivastava (2006)
Katakturuk Dolomite unit K1 (Alaska, USA)	> 4	Nularvik Cap Carbonate (end-Cryogenian)	S 0-15°	Macdonald, McClelland et al. (2009)
Keele Formation (NW Canada)	≤ 5[c]	Ice Brook diamictite (end-Cryogenian)	S 0-15°	Day et al. (2004)
Kunihar Formation, Simla Group (Lesser Himalaya, India)	2-24[c]	Blaini Group (end-Cryogenian)	N 0-15°	Thorie et al. (2018)
Tayshir Member, Tsagaan Oloom Formation (Mongolia)	> 5[c]	Khongoryn diamictite (end-Cryogenian)	N 0-15°	Macdonald, Jones et al. (2009)
Trezona Formation (Australia)	≤ 16	Elatina Formation (end-Cryogenian)	N 0-15°	Singh (1987)

Yankaninna Formation and Weetootla Dolomite (Australia)	≤ 10[c]	Elatina Formation (end-Cryogenian), not directly overlying	N 0-15°	Fromhold and Wallace (2011)
Byng Formation, Upper Miete Group (Alberta, Canada)	≤ 4.5	Unconformably overlain by Cambrian McNaughton Formation (possibly Ediacaran during unconformity?)	S 30-45°	Teitz and Mountjoy (1989)
Johnnie Formation, Rainstorm Member (California, USA)	3.5 (maximum 12)[c]	Incised valley putatively associated with Ediacaran glaciation	S 30-45°	Trower and Grotzinger (2010)
Kalancha Formation (Patom Basin, Siberia)	≤ 25	Zherba Formation (possibly Ediacaran based on C isotope correlations by Pelechaty, 1998)	S 15-30°	Petrov (2018)
Upper Wyman Formation and basal Reed Dolomite (California, USA)	≤ 5	Contemporaneous with Rainstorm Member? (Ediacaran)	S 30-45°	Zenger (1976)

[a]Grain size data from Sumner and Grotzinger (1993) except where otherwise noted. Some examples listed in a recent compilation of giant ooid deposits by Thorie et al. (2018) with grain sizes not substantially > 2 mm are not included because those are not giant ooids, by definition, and their relatively small grain sizes are not useful for differentiating between different scenarios (Figure 1).

[b]Paleolatitudes from compilation by Hoffman and Li (2009).

[c]Grain size data from reference listed in "Reference(s)" column.